



# ANSI/AWS A5.1-91 E6013 Rutile Electrodes: The Effect of Calcite

*All-weld-metal mechanical properties and microstructure, arc stability, and operational characteristics were investigated*

BY N. M. R. DE RISSONE, J. P. FARIAS, I. DE SOUZA BOTT, AND E. S. SURIAN

**ABSTRACT.** This study is part of a program to obtain fundamental knowledge about rutile electrodes, of which information is scarce in international welding literature. In this investigation, three rutile-coated electrodes of the ANSI/AWS A5.1-91 E6013 type were prepared by increasing calcite (natural calcium carbonate —  $\text{CaCO}_3$ ), at the expense of cellulose and Si-bearing components, in their coatings. This modification produced an increase in the slag basicity, which caused a marked increment in all-weld-metal toughness and slight modifications in operational behavior with a decrease in penetration and width of the weld bead, while maintaining the typical excellent operational characteristics of rutile electrodes. Arc stability studies were also performed. All-weld-metal hardness and tensile properties were measured and metallographic studies undertaken.

## Introduction

During the decade of the 1980s, an important decrease in the use of coated electrodes took place in developed coun-

tries (Ref. 1). On the other hand, in Latin America, almost 80% of deposited weld metal is produced from this type of welding consumable (Ref. 2). In China and India, accompanying the noticeable growth of steel production, a marked increase of covered electrode use has been observed (Ref. 3). Everything seems to indicate the use of covered electrodes will stabilize in around 30% of the deposited weld metal (Ref. 1).

Rutile-coated electrodes of the types ANSI/AWS A5.1-91 E6013 and E7024 (Ref. 4) continue to be required. Large manufacturers have replaced covered electrodes with solid and tubular continuous wires, but smaller ones still use covered electrodes for the following reasons (Ref. 2):

- Simplicity, durability, and low cost of the equipment required
- Possibility of being used in open and closed locations
- The relative ease of finding welders with the required skill

- Wide range of consumables for most applications, which is a function of the quick setup fabrication

- Availability in small units at relatively low cost. (It is generally accepted welding consumables represent 1–2 % of the final cost in overall fabrication).

As for covered electrodes for the deposition of C-Mn steels, a lot of research conducted during the last 20 years has been to increase knowledge of basic covered electrodes of types E7018 (Refs. 5, 6) and E7016 (Refs. 7, 8). This is not the case with rutile electrodes. At present, few papers about this type of consumable have been published (Refs. 9–23).

Since welding consumable manufacturers produce larger quantities of rutile-coated electrodes than basic ones and the rutile type is technically more important than the basic, more complete information about rutile electrodes should be generated for the following reasons:

1) The requirements of international classification societies (ABS, BV, DnV, LRS) establish three grades for the classification of rutile electrodes (Ref. 24) according to the temperature at which 47 J minimum, on average, is obtained from the Charpy V-notch impacts. They are Grade 1 +20°C (68°F), Grade 2 0°C (32°F), and Grade 3 –20°C (–4°F) demanding 33 J minimum for each individual value. Grade 3 is normally required for the naval industry, so it is technically important. Not all covered electrode manufacturers have adequate knowledge to consistently satisfy the requirements of the grades mentioned.

## KEY WORDS

Covered Electrodes  
 Rutile Coating  
 Basic Slag  
 SMAW  
 Calcite Additions  
 Weldability

*N. M. R. DE RISSONE and E. S. SURIAN are with the Center for Development and Materials Technology, Facultad Regional San Nicolás, National Technology University, Buenos Aires, Argentina. J. P. FARIAS is with the Department of Mechanical Engineering and Production, Universidade Federal de Ceará, Fortaleza, Brazil. I. DE SOUZA BOTT is with the Department of Science, Materials and Metallurgy, Pontificia Universidade Católica do Rio de Janeiro, Brazil.*

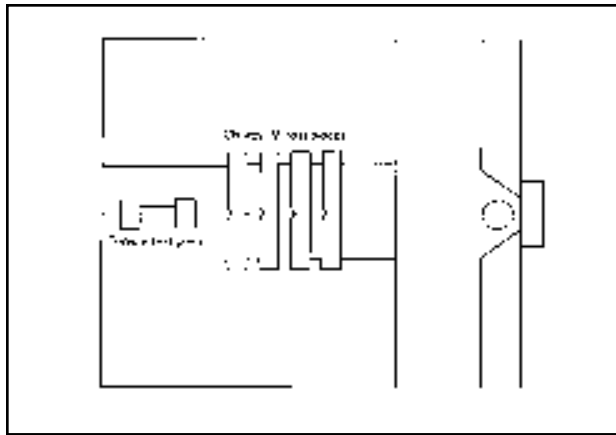


Fig. 1 — All-weld-metal assembly according to ISO 2560 standard.

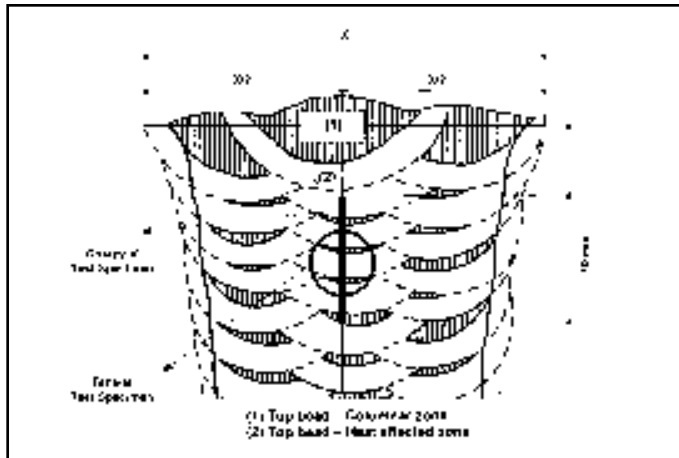


Fig. 2 — Cross section of the all-weld-metal test assembly.

**Table 1 — Coating Composition and Slag Chemical Analysis (wt-%)**

Coating Dry Mix Constituents	5- Calcite	10- Calcite	15- Calcite
	TiO <sub>2</sub>	52	52
SiO <sub>2</sub> + Al <sub>2</sub> O <sub>3</sub> from <sup>(a)</sup>	21	19	13
CaCO <sub>3</sub>	5	10	15
Cellulose	6	3	0
Mn + Fe	15	16	16
K <sub>2</sub> O from <sup>(a)</sup>	1	1	1
	Slag		
CaO	2.3	4.6	7.5
FeO	8.7	8.8	9.3
Al <sub>2</sub> O <sub>3</sub>	4.0	4.0	3.2
SiO <sub>2</sub>	20.8	19.0	14.0
MnO	10.3	12.0	11.1
TiO <sub>2</sub>	51.3	49.3	52.2
Na <sub>2</sub> O	0.3	0.3	0.8
K <sub>2</sub> O	4.8	4.0	3.5
Basicity Index (Ref. 28)	0.35	0.42	0.53

(a) Si-bearing materials: quartz, kaolin, mica, and feldspar.

**Table 2 — Welding Parameters Used for the ISO2560 Test Specimens Welded with DC(-)**

Parameters	5- Calcite	10- Calcite	15- Calcite
	Current (A)	180	200
Voltage (V)	22	19	17
Welding speed (mm/s)	3.7	3.6	3.1
Heat input (kJ/mm)	1.1	1.1	1.2

2) Underwater wet welding has received great interest. Because rutile electrodes are used for this purpose (Refs. 25-26), it is necessary to generate knowledge about them.

3) All-position, flux cored welding

wires are rutile (Ref. 27), as is their slag (it is possible to achieve diffusible hydrogen content under 5 mL/100 g of deposited metal). Basic metallurgical knowledge about rutile electrodes could be obtained in a cheaper and simpler way with covered electrodes, then transferred to tubular wires, as has been done with E7018 basic-coated electrodes.

For these reasons, a research program with covered electrodes of the E6013 type has been developed. This program studied the effect that slag basicity variation, through increasing the calcite coating content, has on the operational characteristics, arc stability, and all-weld-metal properties.

## Experimental Procedure

### Electrodes

Three electrodes with a 4-mm diameter and coating factor (coating diameter: wire diameter) of 1.5 were designed by increasing calcite (natural calcium carbonate-CaCO<sub>3</sub>) from 5 to 15 wt-% at the expense of cellulose and Si-bearing raw materials (quartz, kaolin, mica, and feldspar) in the dry mix. This replacement was undertaken to obtain an increase in basicity of the slag without varying TiO<sub>2</sub> content to maintain the operational characteristics of the rutile electrodes as far as possible. All the electrodes were produced with the same quantity of potassium silicate and the same wire and powder raw material batches. The coating dry mix composition and the slag chemical analyses, with the corresponding basicity indexes (BI) calculated according to Boniszewski (Ref. 28) are shown in Table 1.

In all tables and/or figures, the electrodes will be identified as 5-calcite, 10-calcite, or 15-calcite, depending on the percentage of calcite in the electrode coating (Table 1).

### Operational Properties: Manual Welding

The operational behavior of the three electrodes was studied using an AC-DC 350-A power supply set to AC, alternating current; DC(+), direct current, positive pole to the electrode; and DC(-), direct current, negative pole to the electrode; in flat (F), horizontal fillet (HF), and vertical uphill fillet (VUF) positions; and in vertical downhill (VD) position only on AC.

It was noted as coating calcite increased, it was necessary to increase the current to achieve appropriate operational properties in the flat position. Voltage decreased with increased calcite. Table 2 presents the welding parameters for the flat welding position.

### All-Weld-Metal Test Assemblies

All-weld-metal test assemblies with three passes per layer (a total of nine) according to ISO 2560-73 standard (Ref. 29) (Fig. 1) were manually welded in the flat position, applying DC(-) using the equipment previously mentioned. The base material was ASTM A36. Table 2 shows the welding parameters employed.

### Chemical Composition

Chemical analyses were obtained from both the transversal cut samples extracted from the all-weld-metal coupons, welded on DC(-), and from the weld pads, welded on both AC and DC(+), according to ANSI/AWS A5.1-91 (Ref. 4). The base material was ASTM A36.

### Metallographic Study

The metallographic study was carried out on transverse cross sections of the all-weld-metal test assemblies — Fig. 2. The percentages of columnar and reheated

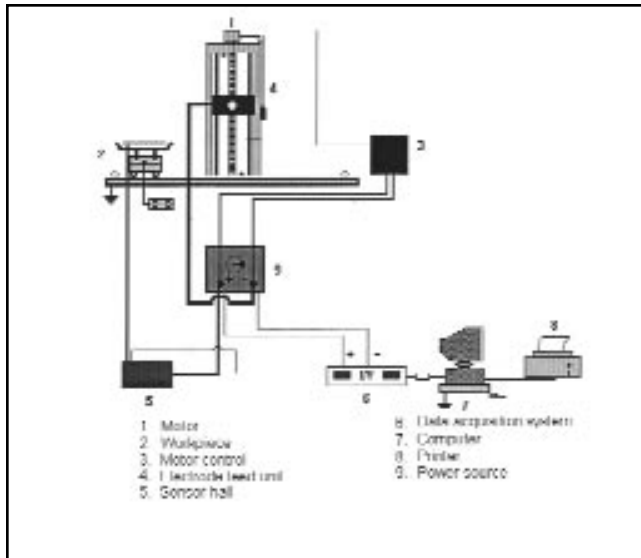


Fig. 3 — Automatic welding equipment.

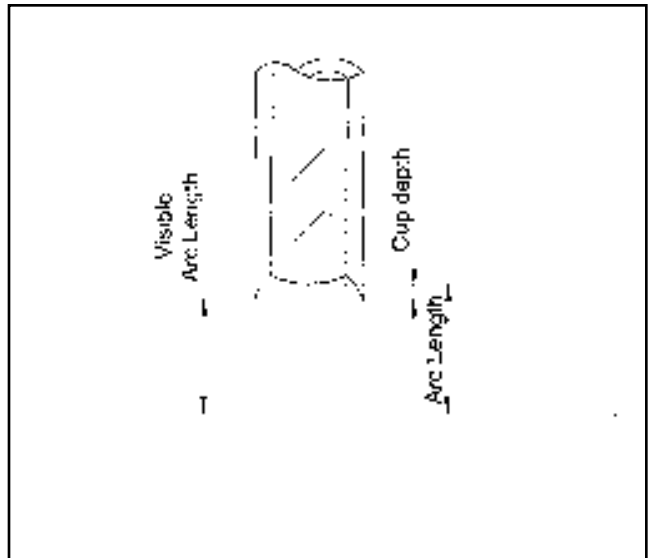


Fig. 4 — The cup, the arc length, and the visible arc length.

zones were measured at 500X at the Charpy V-notch location. The average width of the columnar grain size (the prior austenite grains) was measured in the top bead of the samples at 100X.

To quantify the microstructural constituents of the columnar zones in each weld, 30 fields of 100 points were measured in the top bead at 500X by light optical microscopy, according to Ref. 30. The reheated fine grain size was measured in the heat-affected zone of the top bead, according to the linear intercept method (ASTM E112 standard).

Inclusion analysis was carried out using scanning electron microscopy (SEM). The inclusion chemical composition was determined using energy dispersive spectrometry (EDS) through semi-quantitative measurements. Inclusions with diameters higher than 2 microns were selected. The percentage of each oxide was calculated by stoichiometry from the EDS measurements taking the relative quantities of each element found with the system used (Ti, Al, Si, and Mn), considering their sum was 100%.

### Mechanical Testing

Microhardness was determined on the transverse cross section of the all-weld-metal test assemblies at the Charpy V-notch location (Fig. 2) using the Vickers 1000-g scale.

From each all-weld-metal test assembly, a Minitrac (Ref. 31) test specimen (total length = 55 mm, gauge length = 25 mm, reduced section diameter = 5 mm, ratio of gauge length to diameter = 5:1) was extracted (Fig. 2), as well as sufficient

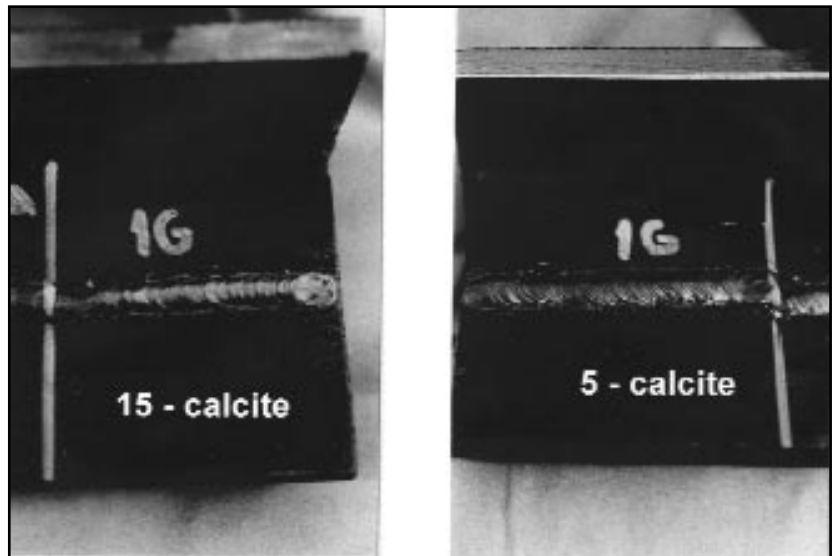


Fig. 5 — Beads obtained in the flat position welding with AC.

Charpy V-notch impact specimens to construct the absorbed energy vs. test temperature curve between 20°C (68°F) and -40°C (-40°F). Tensile property test specimens were tested at room temperature.

### Arc Stability Study

With the electrodes described in Table 1, bead-on-plate welds in the flat position with AC, DC(+), and DC(-) on 50 x 150 x 8 mm ASTM A-36 steel plates were deposited using an automated test bench with computerized data acquisition as shown schematically in Fig. 3. The automated test bench consisted of a 350-A in-

verter, constant power supply with 65 V of open voltage (item 9 of Fig. 3), and an automated welding system developed through a cooperative research project between the Engineering Welding Laboratory (ENGESOLDA) and the Control and Instrumentation Laboratory (LIC) of the Federal University of Ceará, Brazil. This system has a card control (item 3 of Fig. 3) that uses arc voltage to control arc length. Once a voltage variation occurs in the arc, the card control changes the voltage signals sent to the motor (item 1 of Fig. 3), which in turn alters its rotation and consequently the feed velocity of the electrode (item 4 of

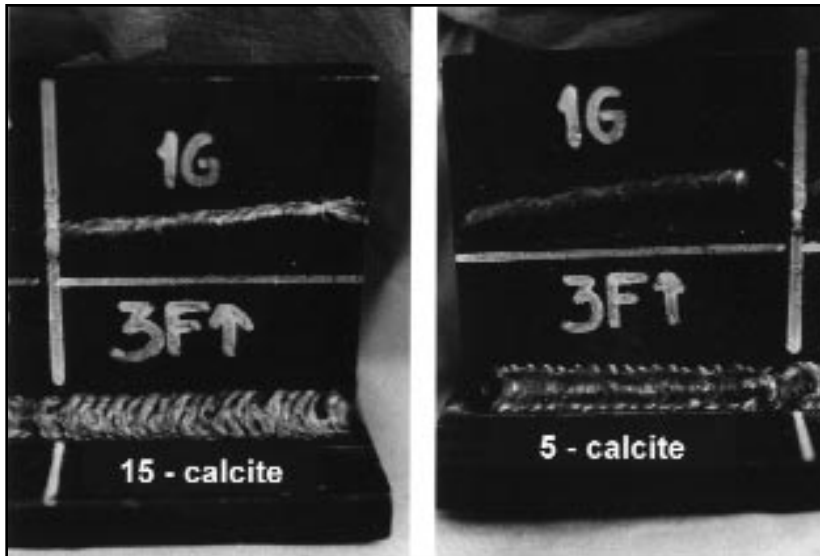


Fig. 6 — Beads obtained in vertical uphill position welding with AC.

ments, are described in the Appendix.

The study of arc behavior was based on a methodology that evaluated arc stability, assessed by considering both the electric charge transfer and metal transfer mechanisms (Refs. 32, 33). All the results were submitted to a variance analysis (Ref. 34), with a confidence level of 95%, for determination of the significance level ( $\alpha$ ) of the analyzed effects. In this study,  $\alpha = 5.0\%$  was considered for comparing average values.

### Electric Charge Transfer Mechanism

The ease of electric charge transfer was evaluated by considering the index  $FE_1$  with DC, and the index  $B^+$  with AC.

$$FE_1 = \frac{1}{E_1} = \frac{2000}{(P_1 - P_0) \cdot t_1} \quad (W^{-1} s^{-1}) \quad (1)$$

$FE_1$  is the inverse of the restriking mean energy after the short circuit occurrence with DC welding. ( $E_1$ ,  $P_1$ ,  $P_0$ , and  $t_1$  are defined in the Appendix.)

$$B^+ = \frac{I_1^+}{U_1^+ \cdot t_1^+} \cdot 1000 \quad (\Omega^{-1} s^{-1}) \quad (2)$$

$B^+$  is the mean rate of increase in electrical conductivity of the interelectrode space during the positive prearc period. ( $I_1^+$ ,  $U_1^+$  and  $t_1^+$  are defined in the Appendix.)

The uniformity of the electric charge transfer was also evaluated by means of the indices  $RE_1$  with DC and  $RB^+$  with AC. They represent the inverse of the relative root-mean-square deviations of the indices  $E_1$  and  $B^+$ .

$$RE_1 = \frac{E_1}{\sigma_{E_1}} \quad (3)$$

$$RB^+ = \frac{B^+}{\sigma_{B^+}} \quad (4)$$

### Metal Transfer Mechanism

In this case, the ease of the metal transfer was evaluated considering the indices  $F_{cc}$  and  $F_{mt}$ . These represent the ease of short circuit occurrence and the ease of drop transfer in the short circuit transition mode, respectively.

$$F_{sc} = \frac{1}{T} \quad (s^{-1}) \quad (5)$$

$$F_{mt} = \frac{1}{t_{sc}} \quad (s^{-1}) \quad (6)$$

**Table 3 — Welding Parameters for the Arc Stability Study**

Electrode	Parameters	Type of Current		AC
		DC(-)	DC(+)	
5- Calcite	Mean	160	164	—
	Root-mean-square	161	164	160
10- Calcite	Mean	160	166	—
	Root-mean-square	161	167	160
15- Calcite	Mean	164	167	—
	Root-mean-square	164	168	160
5- Calcite	Mean	20	20	—
	Root-mean-square	20	21	20
10- Calcite	Mean	19	19	—
	Root-mean-square	19	19	18
15- Calcite	Mean	16	16	—
	Root-mean-square	16	17	17
	Welding Speed (mm/s)	2.9	2.9	2.9

Fig. 3). The welding speed is selected directly by a travel carriage (item 2 of Fig. 3) and kept constant.

The components of the data acquisition system were a sensor hall of 300 A (item 5 of Fig. 3), a signal processing circuit, an A/D converter (item 6 of Fig. 3), a microcomputer (item 7 of Fig. 3), and a printer (item 8 of Fig. 3). This acquisition data system allowed current and voltage reading at programmable frequencies up to 10 Hz at 12 bits per channel.

The simulator controlled the arc voltage in order to weld with the same visible arc length in all experiments. The arc length in turn was controlled via the voltage. The simulator does not measure the arc length but the voltage. The arc length was established for each electrode prior to welding using a calibration curve (voltage vs. arc length). In order to obtain this calibration curve, different current conditions and arc lengths were used. The arc

was projected by means of lenses on a screen with a measurement scale, allowing the arc length to be determined. Once the arc length was determined, the calibration curve indicated the arc voltage value, which in turn was adjusted via the control card of the simulator and kept constant during the whole procedure.

Each experiment, conducted according to the welding parameters listed in Table 3, was undertaken in triplicate. The instantaneous values of arc voltage and current were registered for periods of 6 s, totalling 18 s of acquisition for each combination of electrode/current type. To undertake a behavior analysis, a dedicated software (ANALYSER) was used for treating the instantaneous voltage and current signals acquired (Ref. 32). ANALYSER software determines all the parameters used to evaluate the arc behavior. These parameters, as well as the criteria used to make these measure-

The consistency of metal transfer was evaluated considering the indices  $R_{cc}$  and  $R_{mt}$ . These indices represent the inverse of the relative root-mean-square deviation of the short-circuit period ( $T$ ) and of the short-circuit time ( $t_{sc}$ ), respectively.

$$R_{sc} = \frac{T}{\sigma_T} \quad (7)$$

$$R_{mt} = \frac{t_{sc}}{\sigma_{t_{sc}}} \quad (8)$$

With the exception of the figures related to the electric charge transfer with AC, the rest of the analyses refer to the process involving metallic transfer, that is to say, only short circuits longer than 2.0 ms were considered, because they actually transfer the metallic drop (Ref. 32).

### Cup Depth Measurement

The cup is formed at the arc end of the electrode by the core wire of the electrode melting back inside the still unmelted coating, as indicated in Fig. 4. It was measured using a vernier calliper gauge with 0.01-mm sensitivity.

### Geometry of the Weld Bead

The weld beads obtained from the arc stability study were utilized to measure bead geometry. The transverse cut samples obtained from the weldments were etched with 5% Nital for 5 s to examine the bead geometry. The vernier calliper gauge mentioned previously was employed to measure bead width (BW), penetration (P), and weld reinforcement (WR) of the bead.

## Results and Discussion

### Operational Properties

As the properties studied varied with the changes in the coating calcite content, only 5 calcite and 15 calcite will be mentioned, with the understanding that 10 calcite results lie between the two.

### Arc Characteristics

All electrodes presented a stable arc for each type of current. The 15-calcite arc was softer and visually showed lower penetration than 5 calcite. This is probably due to the presence of cellulose in the 5-calcite coating. The differences mentioned were more notable on DC than on AC. This effect was confirmed through the weld bead geometry determination, as stated previously. In all cases, the arc was well directed.

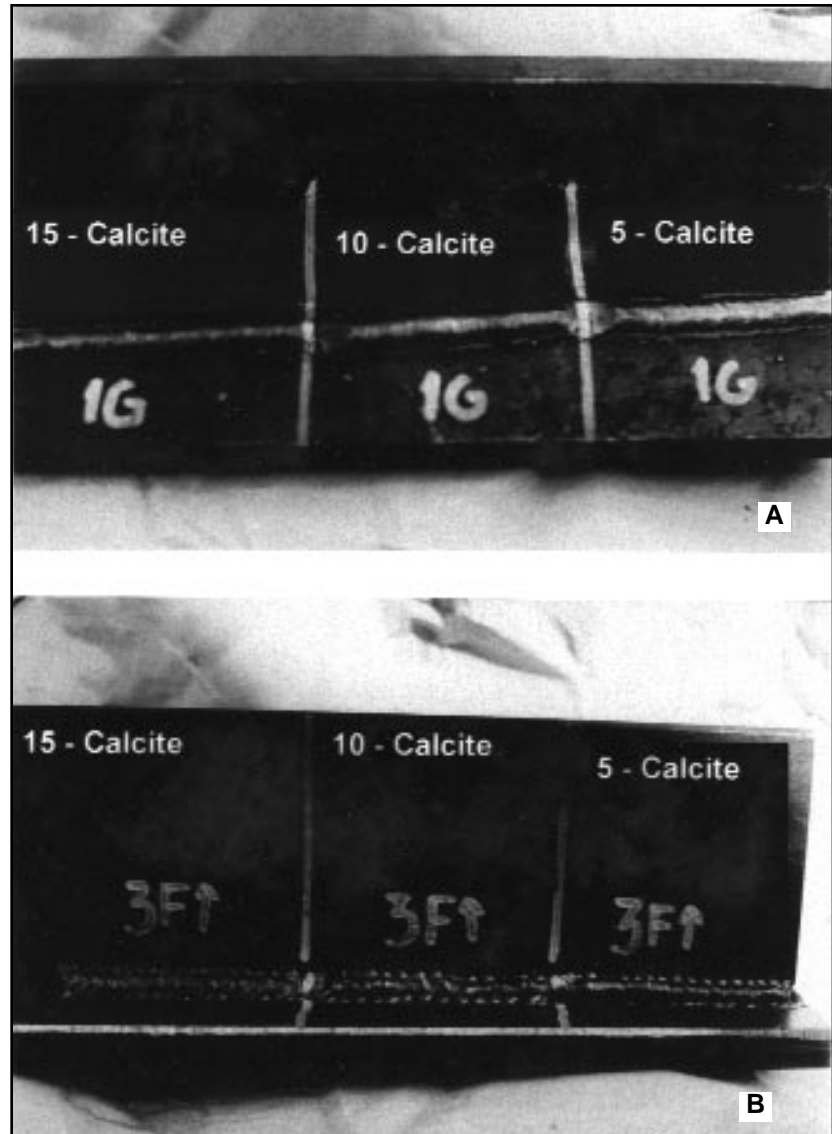


Fig. 7 — Beads obtained welding on DC(+). A — Flat position; B — vertical uphill position.

### Transfer Characteristics

“Spray” transfer was dominant with the three electrodes. In F position, 5 calcite was faster than 15 calcite. However, in VUF, 5-calcite transfer was lower: it took longer to deposit a bead with 5 calcite than with 15 calcite in VUF. In all cases, transfer was faster on AC than on DC.

### Spatter

In general, spatter was moderate, medium sized, and cold (it was possible to remove by simple brushing). For DC(+), 15 calcite presented higher spatter than 5 calcite. This difference is less notable for AC.

### Slag Characteristics

As expected, all the slags were of the rutile type but with slight variations. They all completely covered the beads and, once removed, the bead borders remained clean. The 15-calcite slag was thicker and more abundant than the one deposited by 5 calcite. In VD position, 5-calcite slag did not interfere with the weld pool; the bead was well shaped and deposited quickly. On the other hand, 15-calcite slag was too abundant and tended to interfere with the weld pool. In the last case, the weld was deposited more slowly and bead conformation was irregular. In VUF, the best electrode was 15-calcite. Its slag was the most adequate for this welding position. In this position, the

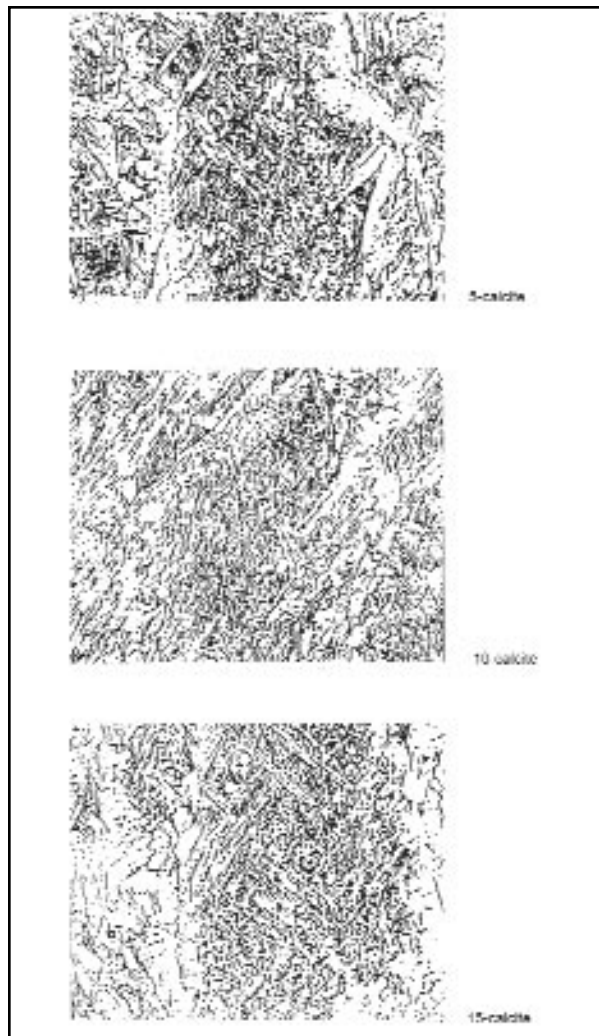


Fig. 8 — Columnar zones (500X).

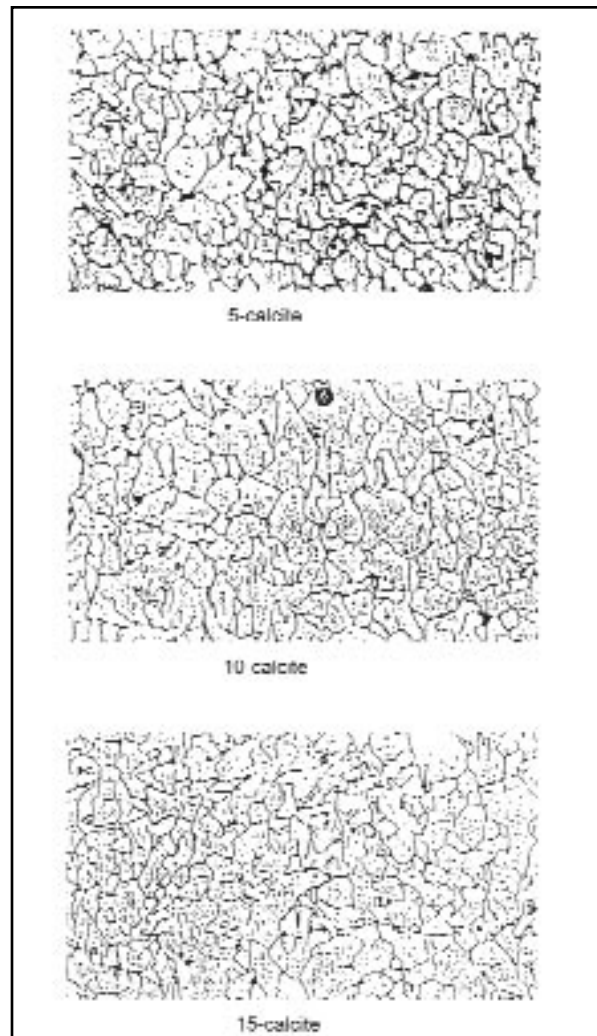


Fig. 9 — Fine reheated zones (740X).

5-calcite slag was too fluid and spilled out. Once again, the behavior mentioned was less marked for AC than for DC.

The slag detachment was better for AC than DC. For AC, all electrodes showed slag self-detachment in F position. In horizontal fillet position, 5 calcite and 10 calcite only presented this effect; 15 calcite did not self-detach but cracked without lifting up. For DC(+) the slag was more difficult to take off, especially with 15 calcite. For this type of welding current, in F position, the slag cracked but did not self-detach.

#### Bead Characteristics

All beads deposited for all types of current were well shaped with fine ripples. In F position, the best bead was achieved with 5 calcite, but, on the contrary, in VU position, the best result was obtained with 15 calcite for all current types. Figures 5, 6, and 7 show these results. In VD position, only 5 calcite could be used, probably due to the elimination

of cellulose from the coatings of 10-calcite and 15-calcite electrodes.

#### Arc Stability

The average values of current, voltage, and welding velocity obtained from the tests for each type of current are shown in Table 3. Since all experiments were made with the same visible arc length, all the differences observed in the arc voltage values as a function of the increase in slag basicity should be due to the variation of both the physical characteristics of the arc atmosphere and the cup depth. The variation of cellulose and  $\text{SiO}_2$  contents (Table 1) must have been the major influence in the increase of the ionization potential on the arc atmosphere.

According to Pokhodnya, *et al.* (Ref. 35),  $\text{SiO}_2$  increases the electron work function, thereby reducing the amount of electrons emitted from the cathode. Additionally, with increasing amounts of gases evolving from the cellulose, the concentration percentage of ionized par-

ticles of potassium, sodium, and their compounds is reduced (Ref. 36). The mean ionization potential of the gaseous atmosphere of the arc is increased because the ionization potential of gases such as  $\text{CO}$ ,  $\text{CO}_2$ ,  $\text{H}_2\text{O}$ , and their dissociated products is high, sometimes as much as four times greater than the ionization potential of potassium or sodium (Ref. 36). As a result of these effects, the arc voltage decreases with the decrease in the cellulose and  $\text{SiO}_2$  contents. The importance of the basic oxides, of low work function, regarding the good operational behavior of the arc should also be mentioned, especially when welding with alternating current, when the current reaches very low values during the polarity inversion, due to the fact the emission properties of the slag improve with an increase in the basicity and degree of deoxidation (Ref. 35).

Table 4 shows the average values of cup depth (in mm) and its related variance analysis. There was a decrease of two thirds in the values of cup depth from

**Table 4 — Depth of the Cup and ANOVA Results**

Electrode	Depth of the Cup (mm)		
	DC(-)	DC(+)	AC
5-Calcite	1.70	2.52	2.38
10-Calcite	1.17	1.53	0.92
15-Calcite	0.52	0.67	0.83
$\alpha$ (%)	6.02	0.07	0.85

the most acid to the most basic electrode. This reduction can be seen as an advantage since it makes the arc reopening by short circuit easier in welding of small beads or spot welds, or it can be seen as a disadvantage because it decreases metallic transfer guiding, exposes the arc, and reduces the possibility of drag welding. This effect can give rise to higher spatter and a larger variation of the arc length, as well as a higher contamination of the weld metal.

Tables 5 and 6 show the results for the quantitative indices and the associated analysis of variance ( $\alpha$ ) for arc stability in DC and AC conditions. Only with direct polarity, DC(-), was the type of electrode observed to have a significant effect on arc stability, as shown by the indices  $FE_1$  and  $F_{mt}$ , where the variance ( $\alpha$ ) was < 5%. The increase of calcite content increased the facility of charge transfer  $FE_1$  in DC(-). However, this increase in calcite content also increased the size of the droplets, reducing the ease of metal transfer given by  $F_{mt}$ . This tendency to increase the droplet size was observed for all three types of current, being more significant for DC(-) ( $\alpha < 5\%$ ), as shown in Tables 5 and 6. These results show the increase in calcite content in electrodes tested under DC current tends to improve the electric charge transfer through the arc, although the metal transfer is worsened. It may be noted, the frequency of metal transfer by short circuit ( $F_{sc}$ ) is not affected in DC ( $\alpha > 5\%$ ). Although coating chemical composition variation changes the short-circuit times, mainly in DC(-), these variations do not affect the frequency, as shown in Table 5. The same did not occur in AC, where metal transfer tended to be more difficult due to the increase in calcite content. On AC, the frequencies of short circuit ( $F_{sc}$ ) exhibited a drastic decrease with the increase of calcite, as shown in Table 6.

Arc stability, for alternating current, evaluated by means of the  $B^+$  and  $RB^+$  indices increased with calcite content, as it did for continuous current (index  $FE_1$ ), proving the increase in slag basicity also increases the charge transfer through the electric arc.

The increase in calcite content associ-

**Table 5 — Results of Arc Stability on DC**

Electrode	Type of Current	Charge Transfer		Metal Transfer			
		Facility $FE_1$ (W.s) <sup>-1</sup>	Regularity RE1	Facility $F_{sc}$ (s <sup>-1</sup> )	$F_{mt}$ (s <sup>-1</sup> )	Regularity $R_{sc}$	$R_{mt}$
5-Calcite	DC(-)	1.15	1.83	4.39	191	1.34	2.22
10-Calcite		1.59	1.73	7.10	134	1.58	2.09
15-Calcite		2.28	1.52	7.04	118	1.53	1.75
	$\alpha$ (%)	1.14	52.70	19.07	0.70	41.93	22.39
5-Calcite	DC(+)	1.48	1.73	6.19	178	1.57	2.62
10-Calcite		1.40	1.60	6.74	153	1.50	2.50
15-Calcite		1.88	1.48	8.38	130	2.03	2.02
	$\alpha$ (%)	33.01	37.19	12.30	6.71	7.98	22.39

$F_{mt}$  (s<sup>-1</sup>) — the ease of metal transfer in the short circuit.  
 $R_{mt}$  — the regularity of metal transfer in the short circuit.  
 $R_{sc}$  — the regularity of short-circuit occurrence (short-circuit frequency).  
 $F_{sc}$  (s<sup>-1</sup>) — the ease of short-circuit occurrence.

**Table 6 — Results of Arc Stability of AC**

Electrode	Charge Transfer		Metal Transfer			
	Facility $B^+$ ( $\Omega^{-1}$ s <sup>-1</sup> )	Regularity $RB^+$	Facility $F_{sc}$ (s <sup>-1</sup> )	$F_{mt}$ (s <sup>-1</sup> )	Regularity $R_{sc}$	$R_{mt}$
5-Calcite	14.879	2.5	11.09	117	1.73	1.81
10-Calcite	18.372	3.3	7.59	112	1.72	1.98
15-Calcite	19.951	4.6	4.93	92	1.78	1.87
$\alpha$ (%)	0.03	0.75	0.08	10.86	96.30	83.64

ated with the decrease of cellulose and SiO<sub>2</sub> in the electrodes analyzed reduced cup depth and arc voltage and improved the conditions of arc reopening in AC (higher indices of  $B^+$  and  $RB^+$ ) and after short circuit in DC(-) (higher indices of  $FE_1$ ), contributing to an improvement in charge transfer through the arc. Also, it impaired the metal transfer due to the increase in short-circuit time (small indices  $F_{mt}$ ) having a more significant effect in DC(-) and AC due to the reduction of the frequency of short circuit ( $F_{sc}$ ).

### Weld Bead Geometry

Table 7 shows results of the weld bead measurements. It can be observed increasing slag basicity produced a reduction in both penetration and bead width for the three types of current used. In all cases, joint penetration and bead width were lower with AC than with DC welding. The slag basicity increase did not seem to have a clear effect on bead reinforcement.

### All-Weld Metal Properties

#### Chemical Composition

Table 8 presents the all-weld-metal chemical composition. In the case of AC and DC(+), the analysis samples were obtained from weld pads and for DC(-)

**Table 7 — Weld Bead Geometry**

	Type of Current	5-	10-	15-
		Calcite	Calcite	Calcite
Bead width (mm)	AC	10.55	10.56	8.82
	DC(+)	11.81	11.43	9.66
	DC(-)	11.03	10.74	9.23
Bead reinforcement (mm)	AC	2.62	2.39	2.24
	DC(+)	2.53	2.30	2.44
Penetration (mm)	DC(-)	2.19	2.10	2.18
	AC	0.78	0.75	0.63
	DC(+)	0.91	0.77	0.65
	DC(-)	0.97	0.88	0.73

from mechanical property test specimens.

The highest transfer of C, Mn, and Si to deposited metal was achieved for DC(-), being slightly lower for DC(+), but markedly lower for AC. This fact agreed with previous results obtained with different types of covered electrodes, E7016 (Ref. 8) and E7024 (Ref. 21). This effect is probably due to the higher oxygen contents found in AC welding with respect to those for DC(+), and DC(-) (Ref. 8).

On the other hand, it was observed that as both slag CaO content and slag basicity increased the deposited metal Si content decreased. This was probably due to two effects: the decrease of coating SiO<sub>2</sub> content as it was replaced with

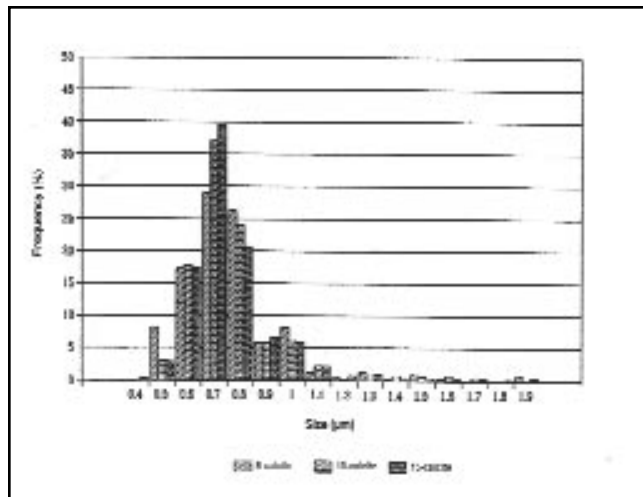


Fig. 10 — Inclusion size distribution.

CaCO<sub>3</sub> and the increase of slag calcium oxide (as calcite increased in the coating, Table 1), which decreased the activity of Si that was transferred to the slag as oxide.

The O values did not present significant variations as had been found in other rutile electrode studies when slag basicity increased (Refs. 10, 22). The N contents were similar to those for DC(-) welding with E6013-type electrodes (Ref. 10) and higher than those achieved with E7024-type electrodes (Refs. 21, 22) (it should be noted the E7024-type electrodes had a thicker coating, and therefore more protection from the atmosphere) and even higher than the N values obtained from basic coated electrodes (Refs. 5-8). This result is probably due to the presence of rutile assisting the transfer of nitrogen by

the formation of TiN, which does not happen in basic coated electrodes (Ref. 37).

The Mn contents were approximately the same for each type of current in spite of the increase in slag basicity, because the Mn powder content of the coatings was adjusted to obtain these results to avoid introducing another variable to the system.

Cr, Ni, Mo, and Ti values were not markedly affected by changes in slag basicity. Nb and V (probably coming from rutile) increased their values as slag ba-

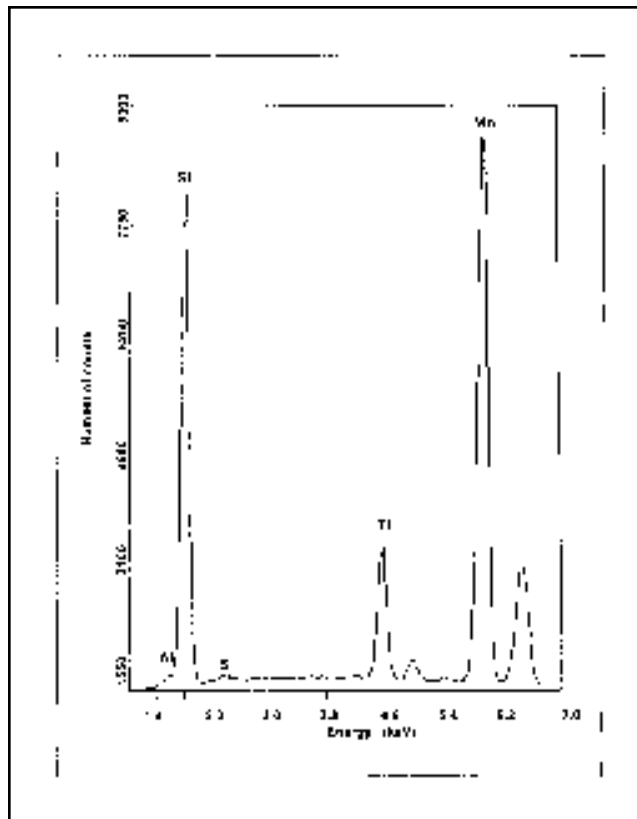


Fig. 11 — Semiquantitative inclusion analysis of 15-calcite deposit.

sicity increased. Al levels were so low it was not possible to observe any effect. The actual chemical composition of the base metal used for both the all-weld-metal test coupons and the weld pads was not taken into account because the samples to be analyzed were extracted from an undiluted area.

**Table 8 — All-Weld-Metal Chemical Composition**

Element (wt-%)	Wire	5-Calcite			10-Calcite			15-Calcite		
		DC(-) (a)	DC(+) (b)	AC (b)	DC(-) (a)	DC(+) (b)	AC (b)	DC(-) (a)	DC(+) (b)	AC (b)
C	0.055	0.051	0.051	0.045	0.046	0.038	0.041	0.043	0.041	0.032
Si	0.09	0.34	0.30	0.21	0.24	0.22	0.14	0.13	0.10	0.05
Mn	0.40	0.46	0.41	0.32	0.48	0.42	0.32	0.41	0.38	0.26
P	0.010	0.010			0.011			0.011		
S	0.018	0.010			0.009			0.009		
Elements in ppm										
Ti	128	150			167			167		
Cr	136	160			169			180		
Ni	382	412			394			402		
Al	< 10	< 10			< 10			< 10		
Nb	< 10	30			50			110		
Mo	103	114			108			108		
V	4	130			162			179		
N	73	172			229			212		
O	136	710			695			734		

a) Chemical analysis from the mechanical property determination coupon.  
 b) Chemical analysis from the weld pad.

**Table 9 — Percentage of Columnar and Reheated Zones**

Test	Columnar Zone (%)	Reheated Zone (%)		
		Fine Grain	Coarse Grain	Total
5-Calcite	8	57	35	92
10-Calcite	27	54	19	73
15-Calcite	35	48	17	65

**Table 11 — Fine Reheated Zone Grain Size**

Test	Diameter (μm)
5-Calcite	8.39
10-Calcite	8.68
15-Calcite	8.41

### Metallographic Study

#### General

The percentage values of columnar and reheated zones at the Charpy V-notch location are shown in Table 9. The three electrodes were used with the same heat input. The 15-calcite electrode presented lower penetration resulting from the elimination of cellulose from the coating. This caused an increase of the columnar zone size at the expense of the reheated one.

#### Columnar Zone

Table 10 shows the microstructural composition of the columnar zone in which the components were quantified according to Ref. 31. There seems to be a slight increase in the acicular ferrite content in the 15 calcite, but the difference was not significant.

The average width of the columnar grains (the prior austenite grains) in the as-deposited weld metal of the final passes is shown in Table 10. The values obtained were very similar. Figure 8 shows typical microphotographs of the columnar zones of the three electrodes.

#### Reheated Zone

Values achieved from measurement of the reheated grain size (ASTM E112 Method) of the fine reheated zone are presented in Table 11. They did not show any significant difference, as can be seen in micrographs of these regions in Fig. 9.

#### Inclusions

In Figure 10, it can be seen the aver-

**Table 10 — Microstructural Composition of the Columnar Zone and Prior Austenite**

Test	AF	PF (G)	PF (I)	PF Total	FS (A)	FS (NA)	FS Total	Width (μm)
5-Calcite	28	42	2	44	25	3	28	112.3
10-Calcite	26	40	2	42	29	3	32	104.1
15-Calcite	32	42	2	44	21	3	24	121.7

AF: Acicular ferrite; PF (G): Grain border primary ferrite; PF (I): Intragranular primary ferrite; FS (A): Ferrite with second phase, aligned; FS (NA): Ferrite with second phase, not aligned; Width: Average width of prior austenite grains.

**Table 12 — Inclusion Composition and Volumetric Fraction**

	5-Calcite	10-Calcite	15-Calcite
Al <sub>2</sub> O <sub>3</sub> % <sup>(a)</sup>	2	1.5	1.5
SiO <sub>2</sub> % <sup>(a)</sup>	48	46	43.5
TiO <sub>2</sub> % <sup>(a)</sup>	14	8.5	10
MnO % <sup>(a)</sup>	36	44	45
Volumetric fraction (%)	0.98	1.08	0.82

(a) Percentage calculated by stoichiometry from the EDS (energy dispersive spectrometry) measurements.

**Table 13 — Microhardness Measurements**

Microhardness (HV1000g)	5-Calcite	10-Calcite	15-Calcite
Columnar zone	189	185	182
Reheated zone fine grain	189	181	176
Reheated zone coarse grain	199	186	185
Average microhardness	192	183	179

**Table 14 — All-Weld-Metal Tensile Property Measurements**

Property Requirements	5-Calcite	10-Calcite	15-Calcite	AWS
Elongation %	22	26	24	17 min.
Yield strength (N/mm <sup>2</sup> )	533	481	463	331 min.
Tensile Strength (N/mm <sup>2</sup> )	603	556	541	414 min.

age size of inclusions is 0.7 mm for the three weld metals. Inclusions larger than 1 mm were not present in significant quantities. The 15-calcite electrode presented less scatter in the inclusion size. Table 12 shows the inclusion volume fractions measured with the SEM. The electrode with the highest slag basicity, 15-calcite, presented the lower volume fraction of inclusions, but there were no important differences among the values obtained with the three electrodes.

Table 12 also presents the approximate inclusion chemical compositions. It was observed that as the coating calcite increased, SiO<sub>2</sub>, TiO<sub>2</sub> and Al<sub>2</sub>O<sub>3</sub> inclusion contents decreased and MnO increased. CaO was not found in the inclusions. Figure 11 shows, as an example, the semi-quantitative inclusion chemical analysis results from 15-calcite, all weld metal.

### Mechanical Properties

#### Microhardness Measurements

Table 13 shows microhardness values obtained from different zones in the Charpy V-notch location. It was observed that as slag basicity increased, the microhardness values decreased in each zone, probably due to the decrease of C and Si.

Weighted averages were calculated taking into account the percentages of columnar and recrystallized zones (Table 9). The averages obtained showed the same trend: microhardness decreased with increments in slag basicity.

#### Tensile Properties

Table 14 presents tensile property results of all weld metals. A decrease in ten-

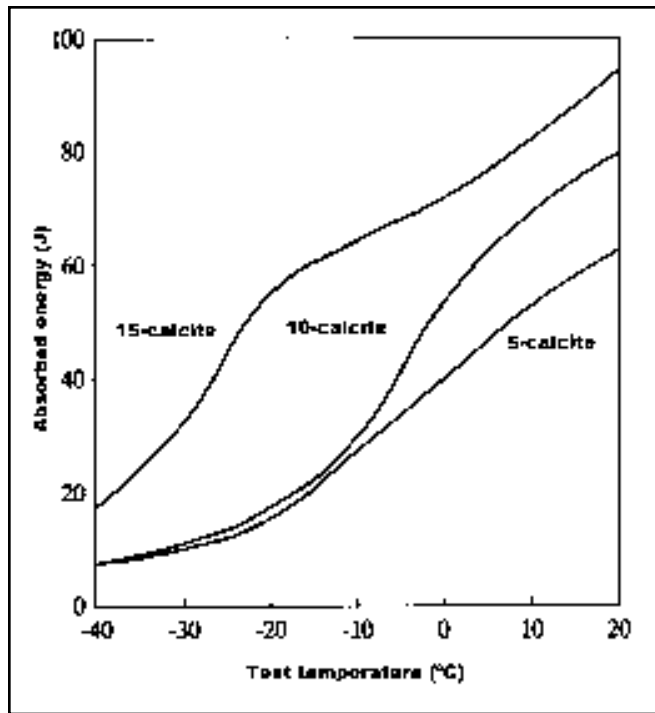


Fig. 12 — Charpy V-notch impact results for the three all-weld-metal samples.

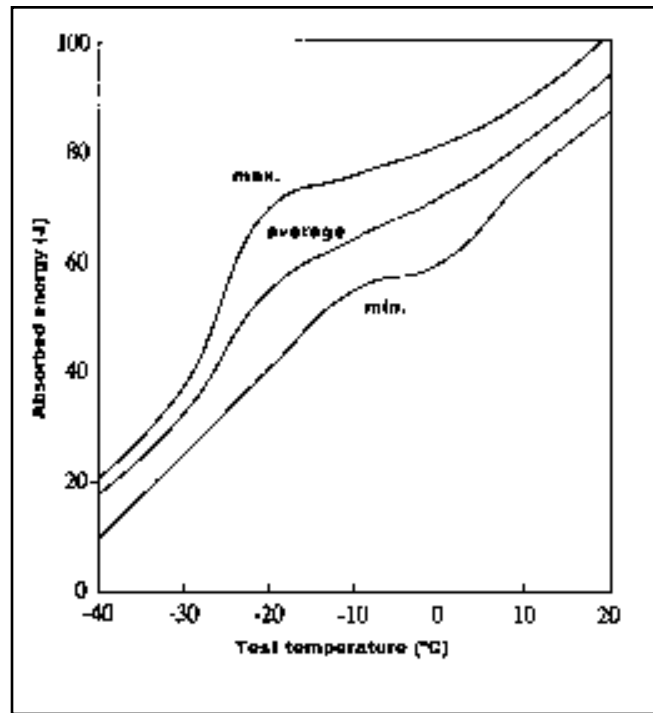


Fig. 13 — Scatter band of Charpy V-notch impact results for 15 calcite.

**Table 15 — All-Weld-Metal Charpy V-Notch Impact Test Results**

Test Average Temp (°C)	5-Calcite		10-Calcite		15-Calcite	
	Charpy V (J)	Average (J)	Charpy V (J)	Average (J)	Charpy V (J)	(J)
-40	10-9-5-6	8	10-7-7-6	8	9-20-20	16
-30	7-12-11-10	10	10-8-20-10	12	30-35-35-25	31
-20	25-30-12-15	21	22-15-15-17	17	70-62-55-61	61
-10	20-25-25-36-24	26	15-22-62-59-25-20	34	61-65-65-50	72
0	35-46-43	41	50-39-75-30-55	50	60-66-80	69
20	55-69-70	65	72-82-89	81	102-89-99	97

sile and yield strengths were observed as Si content of the weld decreased accompanied by a decrease in hardness. All are within the expected ranges for this type of deposit and satisfy AWS E6013 requirements.

### Toughness Results

Charpy V-notch values are presented in Table 15. The absorbed energy vs. temperature curves of the three electrodes are shown in Fig. 12. Figure 13 presents the same curve with its scatter band and the curve resulting from the average values achieved at each temperature for the max-

imum slag basicity electrode (15 calcite).

In Figs. 12 and 13 and Table 15, an important improvement in toughness is observed as slag basicity increased. With the 15-calcite electrode, this improvement was so marked it was possible to satisfy the minimal average Register Society requirements of 47 J at -20°C, as well as the 33-J minimum for each individual value. The ANSI/AWS A5.1-91 E7018 toughness requirement of 27 J at -29 °C (Ref. 4) was also achieved with the 15 calcite.

It is generally accepted that toughness is related to several factors (Refs. 5, 6, and 38): nitrogen content, hardness level, tensile properties, type and quantity of in-

clusions, and microstructural characteristics. In this case, the toughness increase does not seem to be accompanied by significant microstructural variations. Only the inclusion chemical compositions varied with slag basicity; however, this variation was not reflected in microstructural changes, as happens when Ti is varied in E7018 electrodes (Ref. 6). So, this increment of toughness appears to be related to the decrease in tensile properties and microhardness values associated with the decrease in deposited metal Si content, which was shown to be detrimental to toughness in this system, as found in Refs. 9, 12, 13, 17, and 18.

### Conclusions

The coating composition of a standard ANSI/AWS A5.1-91 E6013-type electrode was modified by increasing calcite content to incrementally increase slag basicity. As slag basicity increased, the following were observed:

- 1) A slight deterioration of operational properties in the flat position but an improvement in the vertical-up fillet. This effect is less noticeable for AC than DC. Joint penetration and bead width decreased. In general, the rutile electrode operational behavior was maintained, but to obtain good operational properties, it was necessary to increase welding current as basicity increased.

- 2) An improvement of arc electrical

charge transfer and an impoverishment of metal transfer.

3) A decrease in all-weld-metal Si content.

4) No important microstructural changes were observed by optical microscopy.

5) No significant variation in size distribution of inclusions.

6) Modification in the chemical composition of the inclusions, which were not reflected in microstructural changes observed with optical microscopy.

7) A slight decrease in microhardness values.

8) A reduction in tensile property values.

9) A very important increase in toughness properties.

### Acknowledgments

The authors thank Eng. Celina Leal Mendes da Silva (from CEFET-PA, Brazil) and Eng. Vinicius Sales Rocha (from the Universidade Federal de Uberlândia-Brazil) for the weld bead geometry measurement. The authors Ivani de S. Bott and Jesualdo P. Farias wish to thank CNPq and FINEP (both of Brazil) for the financial support.

### References

1. Myazaki, T. 1998. *Flux Cored Wires for Robots*. Hitachi Zosen Corp. Ariabe Works, IIW-IIS Doc XII-1084-88.
2. Taylor, D. S. 1990. The role of MMA welding in 1990. *Welding and Metal Fabrication*, May.
3. Timerman, R., and de Vedia, L. 1991. Welding in Latin America. *International Conference of South African Welding Institute: "Towards Cheaper Welding"*. Pretoria, South Africa.
4. ANSI/AWS A5.1-91. *Specification for Carbon Steel Electrodes for Shielded Metal Arc Welding*. Miami, Fla.: American Welding Society.
5. Evans, G. 1983. Factors affecting the microstructure and properties of C-Mn all-weld-metal deposits. *Weld. Research Abroad*. WRC, 28.
6. Evans, G. 1990. The effect of alloying elements on the microstructure and properties of ferritic all-weld-metal deposits. IIS/IIW Doc. II-A-817-90.
7. Taylor, D. S. 1982. The effect of manganese on the toughness of E7016 type weld metal. *Welding and Metal Fabrication* 50(9): 452-460.
8. Surian, E., and Boniszewski, T. 1992. Effect of manganese and type of current on the properties and microstructure of all-weld-metal deposited with E7016-1 electrodes. *Welding Journal* 71(1): 348-s to 363-s.
9. Boniszewski, T., Evans, G. M., and Hart, P. H. M. 1994. Studies of AWS E6013 rutile electrodes. part 1: effects of calcium carbonate. IIS/IIW-IIS Doc. II-A-931-94 (II-1263-95)
10. Ramini de Rissone, N. M., Bott, I. de S., Jorge, C. F. J., Corvalan, P., and Surian, E.

1997. ANSI/AWS A5.1-91 E6013 rutile electrodes: the effect of Wollastonite. IIW-IIS Doc. II-A-951-95. *Welding Journal* 76(11): 498-s to 507-s.
11. Farias, J. P., Bálamo de S., P. S., and Scotti, A. 1995. AWS E6013 rutile electrodes: the effect of Wollastonite, part 2: on arc stability and economical characteristics. IIW-IIS Doc. II-A-953-95.
12. Boniszewski, T., and Evans, G. M. 1995. Studies of AWS E6013 rutile electrodes, part 2: changes in toughness at constant strength. IIW-IIS Doc. II-1263-95.
13. Boniszewski, T. and Evans, G. M. 1995. Studies of AWS E6013 rutile electrodes, part 3: deoxidation with silicon. IIW-IIS Doc. II-A-948-95.
14. Boniszewski, T. and Evans, G. M. 1995. Studies of AWS E6013 rutile electrodes, part 4: deoxidation with magnesium. IIW-IIS Doc. II-A-949-95.
15. Boniszewski, T., and Malsingh, I. 1995. Studies of AWS E6013 rutile electrodes, part 5: deoxidation with titanium and magnesium. IIW-IIS Doc. II-A-963-95.
16. Boniszewski, T., and Malsingh, I. 1996. Studies of AWS E6013 rutile electrodes, part 6: generation of acicular ferrite. IIW-IIS Doc. II-A-975-96.
17. Edited by T. Boniszewski. 1996. Round robin report electrode 1366 from Doc. II-A-963-95. IIW-IIS Doc. II-A-984-96.
18. Edited by T. Boniszewski. 1996. Modifications of electrode 1366 from Doc. II-A-963-95 using FeTi instead of Ti. IIW-IIS Doc. II-A-991-96.
19. Elvander, J. 1996. Results from testing 1366 electrode. IIW-IIS Doc. II-A-978-96.
20. Elvander, J. 1997. Results from testing 1366 electrode, part two. IIW-IIS Doc. II-A-004-97.
21. Surian, E., Maraniello, E., and Boniszewski, T. 1995. The effect of carbon in E7024 SMAW electrode all weld metal. IIW-IIS Doc. II-A-905-94. *Welding Journal* 74(8): 279-s to 288-s.
22. Surian, E. 1997. ANSI/AWS E7024 SMAW electrode: The effect of coating magnesium additions, part 1: on operational behavior, diffusible hydrogen and all-weld-metal mechanical properties and microstructure. IIW-IIS Doc. II-A-994-96. *Welding Journal* 76(10): 404-s to 411-s.
23. Mendez da Silva, C. L., Surian, E., and Farias, J. P. 1997. Efeito do magnésio metálico sobre o comportamento do arco de eletrodos AWS E7024. XXIII Encontro de Tecnologia da Soldagem, III Congresso do Mercosul. São Paulo, Brasil.
24. *Rules and Regulations for the Classification of Ships*. Lloyd's Register of Shipping, January 1994 ed.
25. Ibarra, S., Olson, D. L., and Grubbs, C. E. 1989. Underwater wet welding of higher strength offshore steels. *OTC* 5889, pp. 277-282, Houston, Tex: 21st OTC.
26. Sanchez-Osio, A., Liu, S., Olson D. L., and Ibarra S. 1993. Underwater wet welding consumables for offshore applications. *12th International Conference of Offshore Mechanics and Arctic Engineering*. Book No. G0679A.
27. Rutile flux-cored wire for vertical hull joints. 1991. IIW Commission XII project. Present status in the use of cored wires for arc welding worldwide, p. 164. R. Boekholt, ICWET.

28. Tuliani, S. S., Boniszewski, T., and Eaton, N. F. 1969. Notch toughness of commercial submerged-arc weld metal. *Welding Met. Fab.*, Ag., 37: 327-339.
29. ISO 2560-1973(E), Covered electrodes for manual arc welding of mild steel and low alloy steel — code of symbols for identification.
30. Guide to the light microscope examination of ferrite steel weld metals. 1988. IIW Doc. IX-1533-88.
31. Schnadt, H. M., and Leinhard, E. W. 1963. Experimental investigation of the sharp-notch behavior of 60 steels at different temperature and strain rates. IIW-IIS Doc. 196-343-63.
32. Farias, J. P. 1993. Metallic Mg as a coating component in C-Mn-Ni electrode, Ph.D. thesis, Universidade Federal de Santa Catarina, Brazil (in Portuguese).
33. Farias, J. P., Quites, A. M., and Surian, E. 1997. The effect of magnesium content on the arc stability of SMAW E7016-C2L/8016-C2 covered electrodes. *Welding Journal* 76(6): 245-s to 250-s.
34. Montgomery, D. C. 1984. *Design and Analysis of Experiments*. Canada: John Wiley & Sons.
35. Pokhodnya, I. K., Makarenko, V. D., Gorpenyuk, V. N., Ponomarev, V. E., Kasatkin, O. G., Taraborkin, L. A., and Milichenko, S. S. 1984. Research into the special features of metal transfer and arc running stability in welding using basic coated electrodes. *Automatic Welding* 4: 39-42.
36. Wegrzyn, J. 1980. The covered electrode arc. *Weld Pool Chemistry and Metallurgy, International Conference*. Cambridge, England: The Welding Institute, pp. 241-250.
37. Blunt, F. J. 1995. Prediction of weld metal area and chemical composition in C-Mn steels: A literature review. IIW Doc. II-A-956-95.
38. Abson, D. J., and Pargeter, R. J. 1987. Factors influencing the as-deposited strength, microstructure and toughness of manual arc welds suitable for C-Mn steel fabrication. IIW-IIS Doc. II-1092-87.

## Appendix

### Definitions of Arc Variables Measured Using ANALYSER Software

#### Variables Determined with DC

$U_1$ :	restriking mean voltage (V)
$I_1$ :	restriking mean current (A)
$t_1$ :	restriking mean time (ms)
$U_0$ :	reference voltage ( $U_0 = 10$ V)
$I_0$ :	reference current (A), the correspondent value of current in the beginning of the arc restriking

These variables are indicated in Fig. A1.

These variables are used to calculate the indices below:

$E_1$	restriking mean energy after short circuit occurrence with DC welding (Ws)
-------	--

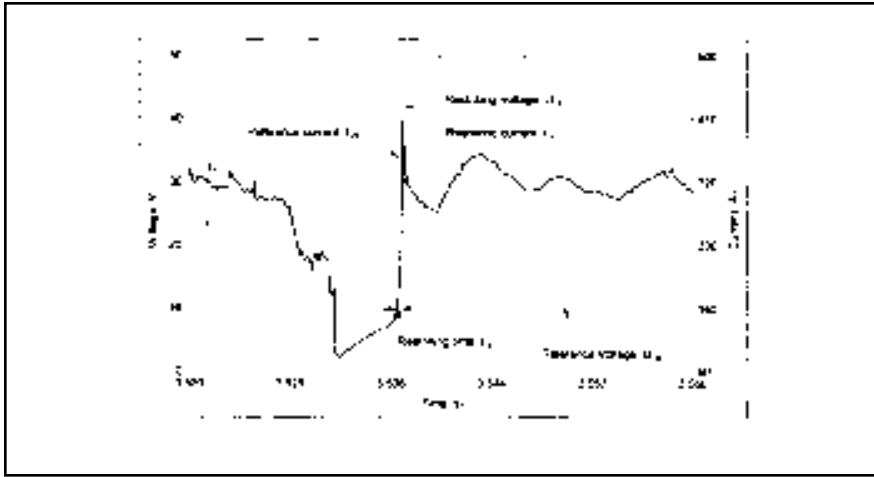


Fig. A1 — The variables determined for DC: reference current  $I_0$ , reference voltage  $U_0$ , restriking voltage  $U_r$ , restriking current  $I_r$ , and restriking time  $t_r$ .

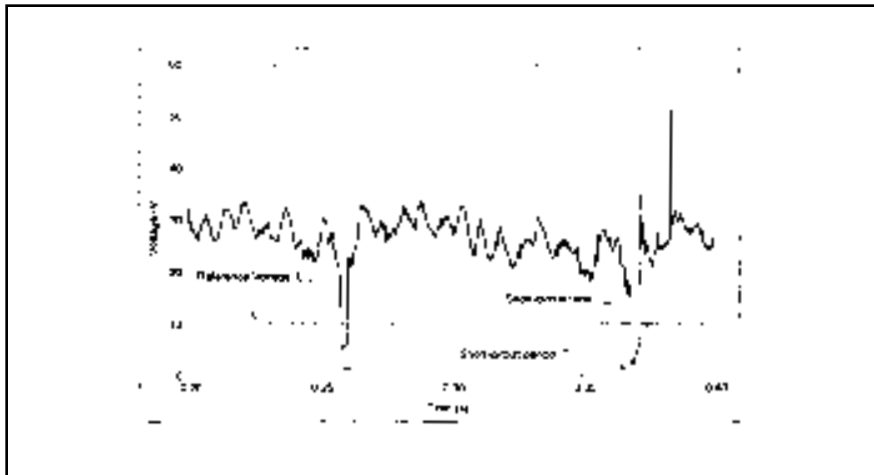


Fig. A2 — Determination of the short-circuit time ( $t_{sc}$ ) and short-circuit period and ( $T$ ).

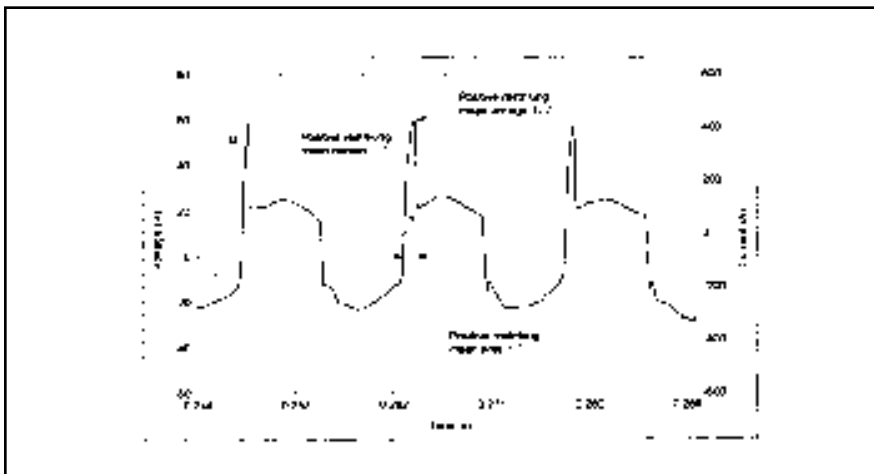


Fig. A3 — The variables determined for AC: positive restriking mean current ( $I_{1+}$ ), positive restriking mean voltage ( $U_{1+}$ ), and positive restriking mean time ( $t_{1+}$ ).

- $P_1$  restriking mean power after short circuit (W)
- $P_0$  reference power (W)

$$E_I = \frac{(P_1 - P_0) \cdot t_1}{(2000)} \quad (A-A)$$

$$P_1 = U_{I_1} \cdot I_{I_1} \quad (A-B)$$

$$P_0 = U_0 \cdot I_0 \quad (A-C)$$

The variable  $E_I$  represents the area over the dynamic behavior ( $P \times t$ ) of the arc power during arc restriking after the short circuit, which was considered approximately as a triangle.

### Variables Determined with AC and DC

- $I_{rms}$  root-mean-square current (A)
- $U_{rms}$  root-mean-square voltage (V)
- $T$  short-circuit period average (ms)
- $\sigma_T$  root-mean-square deviation of  $T$
- $t_{sc}$  short-circuit time average (ms).
- $\sigma_{tsc}$  root-mean-square deviation of  $t_{sc}$ .

Figure A2 illustrates the determination of the short-circuit period and the short-circuit time with DC.

### Variables Determined Only with AC at the Polarity Change for the Positive Half Cycle

- $U_{1+}$  positive restriking mean voltage (V).
- $I_{1+}$  positive restriking mean current (A).
- $t_{1+}$  positive restriking mean time (ms).

These variables are indicated in Fig. A3.

## REPRINTS REPRINTS

To Order Custom Reprints  
of Articles in the

Welding Journal

Call Denis Mulligan  
at (800) 259-0470

## REPRINTS REPRINTS